


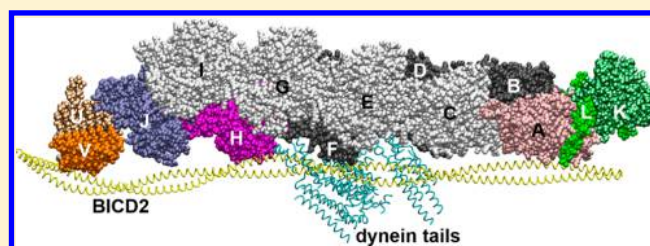
Probing the Energetics of Dynactin Filament Assembly and the Binding of Cargo Adaptor Proteins Using Molecular Dynamics Simulation and Electrostatics-Based Structural Modeling

Wenjun Zheng*

Department of Physics, University at Buffalo, Buffalo, New York 14260, United States

 Supporting Information

ABSTRACT: Dynactin, a large multiprotein complex, binds with the cytoplasmic dynein-1 motor and various adaptor proteins to allow recruitment and transportation of cellular cargoes toward the minus end of microtubules. The structure of the dynactin complex is built around an actin-like minifilament with a defined length, which has been visualized in a high-resolution structure of the dynactin filament determined by cryo-electron microscopy (cryo-EM). To understand the energetic basis of dynactin filament assembly, we used molecular dynamics simulation to probe the intersubunit interactions among the actin-like proteins, various capping proteins, and four extended regions of the dynactin shoulder. Our simulations revealed stronger intersubunit interactions at the barbed and pointed ends of the filament and involving the extended regions (compared with the interactions within the filament), which may energetically drive filament termination by the capping proteins and recruitment of the actin-like proteins by the extended regions, two key features of the dynactin filament assembly process. Next, we modeled the unknown binding configuration among dynactin, dynein tails, and a number of coiled-coil adaptor proteins (including several Bicaudal-D and related proteins and three HOOK proteins), and predicted a key set of charged residues involved in their electrostatic interactions. Our modeling is consistent with previous findings of conserved regions, functional sites, and disease mutations in the adaptor proteins and will provide a structural framework for future functional and mutational studies of these adaptor proteins. In sum, this study yielded rich structural and energetic information about dynactin and associated adaptor proteins that cannot be directly obtained from the cryo-EM structures with limited resolutions.



Dynactin is a large (~1 MDa) complex comprised of more than 20 subunits from 11 different proteins. It works with the cytoplasmic dynein-1 motor to transport various cargoes from a cell's periphery toward the nucleus along microtubules^{1–3} with high processivity.^{4–8} Dynactin is built around a minifilament of actin-related protein 1 (ARP1)⁹ capped at its barbed and pointed ends with a specific length.¹⁰ The formation of a stable complex between dynein and dynactin requires the presence of the N-terminal section of a dimeric adaptor protein named Bicaudal-D2 (BICD2N).^{4,5,11–13} BICD2 belongs to a family of BICD and BICD-related (BICDR) proteins that act as adaptors between dynein and a wide range of cellular cargoes.^{14–16} Mutations of BICD2 are associated with human diseases such as dominant spinal muscular atrophy.^{17–22} BICD2N forms a predominantly coiled-coil homodimer²³ that contains binding sites for dynein and dynactin.^{11,12} The C-terminal section of BICD2 binds to cargo-associated proteins.^{24,25}

On the basis of electron microscopy (EM) studies, schematic models for the dynactin architecture^{26–30} and dynactin–dynein interactions^{4,5,31} were developed, but many molecular details remain obscure because of the limited resolution. High-resolution structural information is largely unavailable for dynactin except for a few crystal structures of small components

and domains of dynactin.^{32–34} As for the BICD proteins, only two high-resolution structures are available for the C-terminal region of the *Drosophila* BICD³⁵ and the mouse BICD1.³⁶ Because of the lack of high-resolution structural information, many outstanding questions remain. For example, how is the dynactin filament assembled from ARP1s, actin, and various capping proteins with a specific length? How do BICD2N and related adaptor proteins interact with dynactin and dynein?

Thanks to recent progress in cryo-EM technology, a high-resolution structure of the dynactin complex has been determined (at a resolution of 4 Å overall and 3.5 Å in the filament).³⁷ The new structure unambiguously determined the composition of the dynactin filament with eight ARP1 subunits (chains A–G and I) and one β -actin (chain H), which is capped by ARP11²⁹ (chain J), p62 (chain Y), p25 (chain V), and p27 (chain U) at the pointed end and a CapZ $\alpha\beta$ dimer (chain K and chain L) at the barbed end³⁷ (see Figure 1a). Among the family of actin-related proteins, ARP1 is the most similar to actin (with a 54% sequence identity), so it is able to form actin-like filaments and bind with β -actin and actin-

Received: October 2, 2016

Revised: December 10, 2016

Published: December 15, 2016

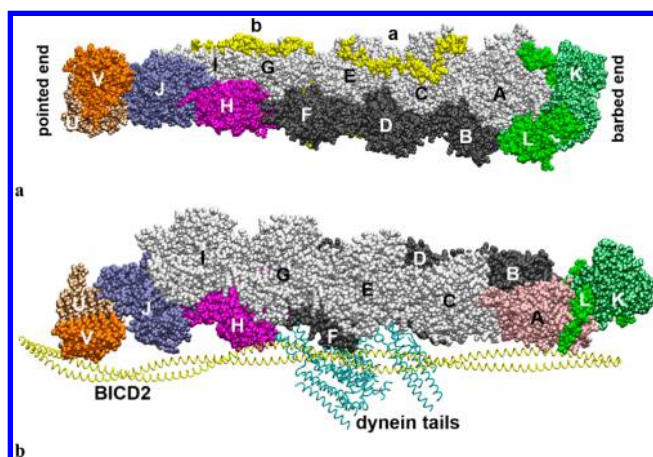


Figure 1. Structural architecture of (a) the dynactin filament and (b) the dynactin–dynein tail–BICD2 complex. The following color coding is used: light and dark gray for two protofilaments of ARP1 subunits, light green for CapZ α , green for CapZ β , magenta for β -actin, ice blue for ARP11, orange for p25, light orange for p27, yellow for ER1/2 in (a), yellow for BICD2 in (b), and cyan for the dynein tail. The dynactin subunits are labeled by the chain ids (see [Methods](#) for details). In panel b, the main contacts of BICD2 are with p25, β -actin, dynein tails, and ARP1 subunit A (colored pink).

capping proteins like CapZ $\alpha\beta$.³⁸ In the pointed-end complex formed by ARP11, p62, p25, and p27,³⁹ p25 and p27 are not required for filament stability and may be involved in targeting and recruiting various cargoes¹⁰ (e.g., positively charged or hydrophobic residues of p25 may bind with membrane lipids³⁹ or other acidic cargoes⁴⁰). On top of the filament is the dynactin shoulder, which was not resolved in side chains except for four N-terminal peptides of the p50 subunits.³⁷ These largely unstructured peptides, known as extended regions (ERs), are required for ARP1 binding.^{41,42} On the basis of this detailed structure, a model was proposed to explain how a dynactin filament with a defined length is assembled with the help of the capping proteins described above and the ERs.³⁷ Additionally, the structure of a stable dynein tail–dynactin–BICD2N (TDB) complex was determined by cryo-EM at a resolution of 8.2 Å.³⁷ In this complex, a coiled coil of BICD2N runs the length of the filament, where the N (C) terminus of BICD2N lies close to the barbed (pointed) end of the filament (see [Figure 1b](#)). However, the side chains of BICD2N were not resolved at this resolution, so the amino acids of BICD2N that interact with dynactin and the dynein tail remain unknown.

To fully understand the molecular mechanisms of dynactin filament assembly and dynactin– and dynein–BICD2 interactions, it is essential to utilize structure-based simulation and modeling to obtain key structural and dynamic information not directly available from the static structures with limited resolutions. Molecular dynamics (MD) is the method of choice for simulating protein dynamics and energetics with atomic detail in the presence of water and ions.⁴³ Previous MD simulation studies have provided rich structural and dynamic information for an actin filament interacting with a coiled-coil protein named tropomyosin.^{44,45} In the past, MD simulation of a large biomolecular system like the solvated dynactin filament [total of ~581000 atoms (see [Methods](#))] was highly expensive, demanding the use of a massively parallelized or special-purpose supercomputer. Because of recent developments in computing hardware and software (particularly the use of graphics processing units to accelerate MD simulation⁴⁶), one

can now routinely run a MD simulation of a large system (with several hundred thousand atoms) at a speed of several nanoseconds per day on a single computer node. This allows effective sampling of the conformational space of a protein complex by simultaneously running multiple relatively short MD trajectories (tens of nanoseconds).⁴⁷ Such a simulation strategy is appropriate for probing energetics and fast fluctuations of a protein complex in a stable state, although much longer MD simulations (microseconds to milliseconds) are needed to explore slow dynamics such as a structural transition between two stable states.

To probe the energetic basis of the dynactin filament assembly, we exploited MD simulation to analyze the intersubunit interactions among the actin-like proteins (ARP1 and β -actin), various capping proteins (ARP11, p62, p25, p27, and CapZ $\alpha\beta$), and four extended regions of the dynactin shoulder (ER1–ER4). Our simulations revealed stronger intersubunit interactions at the barbed and pointed ends of the filament and between the extended regions and the ARP1 subunits (compared with the interactions between ARP1 subunits), which may energetically drive filament termination by the capping proteins and recruitment of the ARP1 subunits by the extended regions, respectively. Additionally, we modeled the TDB complex structure of the dynein tail, dynactin, and a number of coiled-coil adaptor proteins (such as BICD2) and predicted a key set of charged residues involved in the electrostatic interactions between an adaptor protein and dynein and dynactin. Our modeling is consistent with the previous findings of conserved regions, functional sites, and disease mutations in the adaptor proteins and will provide a structural framework for guiding future functional and mutational studies of these proteins. Our simulation- and modeling-based approach complements the experimental structural biology methods by providing key structural, dynamic, and energetic details critical to the elucidation of dynactin functions.

METHODS

MD Simulation of the Dynactin Filament. We performed MD simulation for the filament portion of a cryo-EM structure of the dynactin complex [Protein Data Bank (PDB) entry 5AFT]. This includes eight ARP1 subunits (chains A–G and I), a β -actin subunit (chain H), an ARP11 subunit (chain J), a CapZ $\alpha\beta$ dimer (chains K and L), a p25 subunit (chain V), a p27 subunit (chain U), and four extension regions of p50 subunits (ER chains a–d). The p62 subunit was not included because its electron densities were not adequately resolved for side chain modeling.³⁷ Although p62 is known to be essential for the integrity of the dynactin filament,³⁹ it is structurally dispensable for the association of p25 and p27 with the rest of the ARP1 filament.⁴⁸ Indeed, as shown by the cryo-EM structure, p25 and p27 pack end-on to ARP11 as a continuation of the bottom protofilament (see [Figure 1a](#)), which is reinforced by p62 that wraps around the ARP11–p25/p27 contact site.³⁷ We used the MODLOOP server⁴⁹ to add missing residues in ARP1 (amino acids 1–6), β -actin (amino acids 1–5), ARP11 (amino acids 1–11, 189–192, 233–238, and 391–417), CapZ α (amino acids 1–6 and 282–286), CapZ β (amino acids 1 and 272–277), p27 (amino acids 1–12 and 181–185), p25 (amino acids 1–17), ER chain a (amino acids 21–36), and ER chain b (amino acids 21–36). Only amino acids 1–20 of ER chains c and d were kept in our model. The hydrogen atoms and other missing atoms were added with

the Visual Molecular Dynamics (VMD) program.⁵⁰ The proteins were immersed in a rectangular box of water molecules extending 10 Å from the proteins in each direction by using the VMD program. To ensure a physiological ionic concentration of 0.15 M and a zero net charge, 349 Na⁺ and 236 Cl⁻ ions were added to the system by the VMD program. The entire system contains ~581000 atoms.

To remove atomic clashes, the system was refined with two rounds of energy minimization using the steepest descent method. First, a 5000-step energy minimization was performed to refine the solvent with harmonic constraints (force constant of 10 kcal mol⁻¹ Å⁻²) applied to all protein atoms, and then a 5000-step energy minimization was conducted to refine the protein side chains with harmonic constraints (force constant of 10 kcal mol⁻¹ Å⁻²) applied to the backbone atoms only. The system was gradually heated to room temperature (300 K) over 300 ps by MD simulation with harmonic constraints (force constant of 1 kcal mol⁻¹ Å⁻²) applied to the C α atoms to preserve the global protein conformation. Then the system was equilibrated for 1 ns by MD simulation in the constant-temperature, constant-volume ensemble with the same constraints that were used for heating. Finally, a 50 ns MD simulation was performed in the constant-temperature, constant-pressure ensemble. The Nosé–Hoover method^{51,52} was used to maintain constant temperature (T) of 300 K and constant pressure (P) of 1 atm. The periodic boundary conditions were imposed to eliminate boundary effects. A 10 Å switching distance and a 12 Å cutoff distance were used for nonbonded interactions. The particle mesh Ewald (PME) method⁵³ was used to accurately calculate long-range electrostatic interactions without a cutoff. The SHAKE algorithm⁵⁴ was used to constrain the bond lengths of hydrogen-containing bonds, which allows a larger time step of 2 fs for MD simulations. The atomic coordinates of the system were saved for subsequent analysis every 50 ps during MD simulations. The energy minimization and MD simulation were conducted with the NAMD MD simulation program⁵⁵ using the CHARMM27 force field⁵⁶ (with the CMAP corrections⁵⁷) and the TIP3P water model.⁵⁸

MD-Based Energetic Analysis. We used the following criteria to identify a hydrogen bond (HB) between two polar non-hydrogen atoms (i.e., acceptor and donor): the donor–acceptor distance is <3.5 Å, and the donor–hydrogen–acceptor angle is >120°. A salt bridge (SB) is identified between two oppositely charged residues if the distance between their charged O/N atoms is <4 Å. We used the VMD program⁵⁰ to identify and calculate the occupancy of each HB or SB within a structural ensemble (defined as the probability that this HB or SB is formed in the ensemble). We considered only those HBs or SBs with an occupancy of ≥ 0.3 .

We used the NAMD energy plugin of the VMD program to calculate the van der Waals (VDW) interaction energy between adjacent dynactin subunits. A 10 Å switching distance and a 12 Å cutoff distance were used for the VDW interactions. The CHARMM27 force field was used for the VDW parameters.

We used the measure command of the VMD program to calculate the solvent accessible surface area of each dynactin subunit in isolation (denoted a_i for subunit i) and in complex (denoted A_{ij} between subunits i and j) and then calculated the contact surface area between each pair of adjacent subunits as $(a_i + a_j - A_{ij})/2$.

Coiled-Coil Threading. We threaded the sequence of an adaptor protein along the coiled-coil backbones of BICD2 in

chains 5 and 6 of the TDB structure (PDB entry 5AFU), where we assigned the amino acid at position $S + 1$ (1) of the given sequence to position 1 ($1 - S$) of chains 5 and 6, if the position shift S is positive (negative). The following adaptor proteins were modeled: mouse BICD2 (sp|Q921C5.1), mouse BICD1 (sp|Q8BR07.2), *Drosophila* BICD (sp|P16568.2), mouse BICDR1 (sp|A0JNT9.1), mouse HOOK1 (sp|Q8BIL5.2), mouse HOOK 2 (sp|Q7TMK6.3), and mouse HOOK3 (sp|Q8BUK6.2). The S ranges for these adaptor proteins were chosen according to the predicted coiled-coil regions (from the UNIPROT database): [0, 100] for BICD2, [-10, 90] for BICD1 and BICD, [50, 150] for BICDR1, and [100, 200] for the HOOK proteins. For a given S , we assessed the compatibility of the threaded sequence with the coiled-coil structure as follows. (1) We predicted the heptad positions ($abcdefg$) of the given sequence using the COILS program⁵⁹ and recorded the core a/d positions predicted with at least 50% probability as “sequential core positions” of the coiled coil. (2) For residue n in chain 5 (or 6) of 5AFU ($n = 1, 2, \dots, 275$), we calculated the minimal C α –C α distance (d_n) between this residue and chain 6 (or 5), sorted them from low to high, and kept the top 2/7 positions as “structural core positions” of the coiled coil. (3) We calculated a coiled-coil packing score Score_{CC} defined as the fraction of “sequential core positions” that are also “structural core positions” and plotted Score_{CC} as a function of S (see Figure S1). In this plot, the peaks correspond to S values for which the threaded sequence is compatible with the coiled-coil structure with optimal matching between the “sequential core positions” and the “structural core positions”.

Electrostatic Energy Calculation. We modeled side chain atomic coordinates in the adaptor protein, p25, p27, ER1–4, and dynein tails using the SCWRL4 program.⁶⁰ The two human dynein tails (sp|Q14204.5) were modeled from an X-ray structure of the yeast dynein tails (PDB entry 5AFR) based on their sequence alignment (with a 43% sequence similarity). We calculated the electrostatic interaction energy between the adaptor protein and dynactin and dynein by summing over all pairs of charged residues (D, E, K, or R) as follows:

$$E = \sum_{i,j} \frac{q_i q_j}{d_{ij}} e^{-d_{ij}/d_D}$$

where q_i (q_j) = ± 1 is the charge of residue i (j) from the adaptor protein (dynactin and dynein), d_{ij} is the distance between the side chain centroids of residues i and j , and $d_D = 3.04/\sqrt{I} = 7.8$ Å is the Debye length for electrostatic screening in an electrolyte solution with an ionic strength (I) of 0.15 M.

Then we plotted E as a function of S (see Figure S1) to identify S values that minimize E while satisfying the criterion of being compatible with the coiled-coil structure (see Figure S1). Although E considers only the electrostatic energy, it correlates well with the full binding affinity calculated by the PRODIGY web server⁶¹ [with a Pearson correlation of 0.8 (see Table S1)].

RESULTS AND DISCUSSION

MD Simulation of Intersubunit Interactions in the Dynactin Filament. We performed MD simulation starting from the cryo-EM structure of the dynactin filament (PDB entry 5AFT) in the presence of a box of water molecules and ions (see Methods). To construct a structural ensemble for energetic analysis, three 50 ns MD trajectories were generated and combined (after discarding the initial 10 ns when the

Table 1. Summary of Intersubunit Interactions Based on MD Simulations

subunit pair	no. of HBs (mean \pm standard deviation)	no. of SBs (mean \pm standard deviation)	VDW energy (mean \pm standard deviation) (kcal/mol)	contact area (mean \pm standard deviation) (\AA^2)	
first protofilament	A-C	10.9 \pm 1.9	1.9 \pm 0.7	90.8 \pm 13.4	1176 \pm 84
	C-E	8.6 \pm 2.4	1.2 \pm 0.8	92.3 \pm 10.6	1174 \pm 72
	E-G	9.9 \pm 1.9	1.4 \pm 0.6	88.5 \pm 9.7	1113 \pm 66
	G-I	9.6 \pm 2.1	1.0 \pm 0.5	96.2 \pm 9.6	1152 \pm 51
second protofilament	B-D	9.2 \pm 2.6	1.0 \pm 0.6	89.6 \pm 8.8	1117 \pm 49
	D-F	11.8 \pm 2.8	1.8 \pm 0.6	94.4 \pm 10.6	1199 \pm 61
	F-H	7.7 \pm 1.9	0.7 \pm 0.6	85.3 \pm 12.6	1090 \pm 101
barbed end	A-L	15.4 \pm 7.1	4.0 \pm 1.5	84.7 \pm 15.2	1374 \pm 159
	A-K	8.3 \pm 2.3	3.0 \pm 1.1	24.6 \pm 5.3	490 \pm 33
	B-K	8.9 \pm 2.9	1.7 \pm 1.1	53.7 \pm 13.7	908 \pm 170
pointed end	H-J	10.7 \pm 2.4	3.6 \pm 0.9	98.4 \pm 13.1	1455 \pm 98
	I-J	18.8 \pm 4.0	5.1 \pm 1.4	72.3 \pm 12.5	1432 \pm 138
	J-U	5.1 \pm 2.3	1.3 \pm 0.7	19.0 \pm 8.2	378 \pm 105
	J-V	3.1 \pm 1.8	0.7 \pm 0.6	30.8 \pm 11.4	457 \pm 159
ERs-related	a-C	19.0 \pm 3.8	3.7 \pm 1.2	91.7 \pm 17.3	1483 \pm 193
	a-E	12.4 \pm 3.2	3.9 \pm 1.0	40.6 \pm 14.8	801 \pm 194
	a-A	1.6 \pm 1.8		10.2 \pm 3.8	195 \pm 56
	b-G	23.1 \pm 3.1	4.9 \pm 1.1	117.3 \pm 12.3	1838 \pm 104
	b-I	12.8 \pm 2.1	3.8 \pm 0.9	50.0 \pm 11.2	879 \pm 102
	b-F	5.9 \pm 2.6	1.7 \pm 1.1	20.6 \pm 9.0	437 \pm 105
	b-E	3.5 \pm 2.2	0.8 \pm 0.8	22.9 \pm 7.2	407 \pm 78
	c-D	8.4 \pm 2.6	2.5 \pm 1.1	37.7 \pm 12.2	681 \pm 138
	d-F	10.7 \pm 2.4	2.8 \pm 1.0	47.9 \pm 10.5	818 \pm 148

system undergoes equilibration). We then conducted an ensemble-based analysis of the intersubunit interactions [including hydrogen bonds (HBs), salt bridges (SBs), and van der Waals (VDW) energy (see [Methods](#))] to understand the energetic basis of the filament assembly and capping process. Despite the large size of the dynactin filament (with 4921 residues), 50 ns seems to be sufficient to equilibrate the system (see [Figure S2](#)) and sample the dynamic intersubunit interactions. We have verified the robustness of the results of the analysis by using a different truncation of the MD trajectories (see [Table S2](#)).

Within the dynactin filament, there are two protofilaments wrapping around each other. They are formed by subunits/chains ACEGI and BDFH, and all but chain H are ARP1 (see [Figure 1a](#)). In each protofilament, the intersubunit interactions feature 8–12 HBs, 1–2 SBs, a VDW energy of 85–96 kcal/mol (in absolute value), and an intersubunit contact surface area of $1.1\text{--}1.2 \times 10^3 \text{ \AA}^2$ (see [Table 1](#)). Similar to an actin filament, the flexible loop of subdomain 2 [including residues K43, V45, V47, M48, A49, L52, H65, and R66 (see [Tables 2 and 3](#))] is involved in forming intersubunit HBs and SBs along the long pitch helix of the dynactin filament.²⁶

At the barbed end, the protofilaments are capped by a CapZ $\alpha\beta$ dimer (chains K and L) via ~ 15 HBs and ~ 4 SBs between ARP1 subunit A and CapZ β (chain L), which are reinforced by ~ 8 HBs and 2 or 3 SBs between ARP1 subunits AB and CapZ α (chain K) (see [Table 1](#) and [Figure 2a](#)). The number of these capping HBs/SBs is greater than the number of intersubunit HBs/SBs within the ARP1 filament (see above), which explains why the barbed-end capping of the ARP1

filament by CapZ $\alpha\beta$ is favored over filament extension,³⁷ allowing CapZ $\alpha\beta$ to serve as a stabilizer of the ARP1 filament.²⁶ These capping interactions involve charged residues R152, E172, R264*, D266*, E270*, E271, K285, D287, D289, R291, and K355* of ARP1. Some of them (labeled with an asterisk) are not conserved in charge between ARP1 and β -actin. This explains why CapZ $\alpha\beta$ binds more strongly with ARP1 than with actin.³⁷ Only a subset of the charged residues mentioned above (in amino acids 266–273) were previously identified by inspecting the static cryo-EM structure,³⁷ supporting the usefulness of MD simulation to fully explore dynamic interactions. The ARP1-binding residues of CapZ $\alpha\beta$ are primarily distributed in the C-terminal helical region [amino acids 220–286 of CapZ α and amino acids 210–277 of CapZ β (see [Tables 2 and 3](#) and [Figure 2a](#))], which is consistent with previous proposals that this region serves as likely points of interaction with the actin/ARP1 filament.^{32,62,63}

At the pointed end, a β -actin (chain H) is incorporated into the lower protofilament (see [Figure 1a](#)). However, our energetic analysis found that β -actin binds more weakly to ARP1 [with slightly fewer HBs and SBs (see [Table 1](#))], so it is not energetically favorable for β -actin to compete with ARP1 for binding at the pointed end. As suggested by Carter et al.,³⁷ the favorable incorporation of a β -actin is due to a concentration of actin much higher than that of ARP1 in cells.⁶⁴ The pointed end of the filament is capped by an ARP11 subunit that forms 11 (19) HBs and 4 (5) SBs with β -actin (ARP1 subunit I) (see [Table 1](#) and [Figure 2b](#)). These capping interactions are stronger than the intersubunit HB and SB interactions within the ARP1 filament (see above), which

Table 2. Summary of Intersubunit Hydrogen Bonds Based on MD Simulations

subunit pair	HB-forming residue pairs
A-C	S209-D289 K43-D287 V45-A175 V47-G173 M48-G173 H65-Y171 R66-D289
C-E	D245-R291 K43-D287 V45-A175 V47-G173 M48-G173 A49-Y148 R66-D289
E-G	D245-R291 K43-D287 V45-A175 V47-G173 M48-G173 A49-Y148 R66-D289
G-I	P244-R292 D245-Q284 D245-R291 D245-R292 K43-D287 V45-A175 V47-G173 M48-G173 A49-Y148 L52-E172 H65-Y171
B-D	S209-D287 P244-R292 D245-R291 K43-D287 V45-A175 V47-G173 M48-G173 A49-Y148 L52-E172 H65-Y171
D-F	D245-R291 K43-D287 V45-A175 V47-G173 M48-G173 A49-Y148 H65-Y171 R66-D289
F-H	D245-R290 V45-A170 V47-G168 M48-G168 H65-Y166 R66-D288
A-L	R152-R269 G173-Q259 F174-Q259 R264-D219 K285-E230 K285-K235 D287-K235 K355-E261
A-K	G269-R266 E270-R266 E271-R260 D289-K166 R291-E200
B-K	D287-R260 D287-V264 D287-R266 F376-K273
H-J	D244-K339 V247-K334 G46-G154 K61-E153 R62-D294 K84-D400
I-J	R199-E145 K200-D386 K200-S99 G202-N58 E277-K403 K43-E276 S70-E276
J-U	D209-R147
J-V	K44-S154 R78-E156
a-C	D29-R66 Q30-E212 A31-E219 E36-K308 E39-G309 S44-D312 E46-R329 E46-I330 E46-A332 A48-A332 A48-Q334 N51-T150
a-E	I12-A332 R14-D312 R14-I330 E16-K319 D18-K327
b-G	D24-R220 E32-R220 E38-K308 E39-G309 E39-G311 S44-D312 E46-R329 E46-I330 E46-A332 I48-A332 N51-A149 K58-G151 D70-R373 F71-R373 S72-R373 S72-F376 D73-R118
b-I	R14-D312 R14-I330 E16-K319 E16-I328 D18-K327
c-D	R14-D312 R14-I330 E16-R329
d-F	R14-D312 R14-I330 E16-K319 K5-R336 D8-K308

Table 3. Summary of Intersubunit Salt Bridges Based on MD Simulations

subunit pair	SB-forming residue pairs
A-C	K43-D287 R66-D289
C-E	K43-D287 R66-D289
E-G	K43-D287 R66-D289
G-I	K43-D287
B-D	K43-D287
D-F	K43-D287 R66-D289
F-H	R66-D288
A-L	D287-K235 R264-D219 K285-E230 K355-E261
A-K	D266-K268 D289-K166 E271-K256 R291-E200
B-K	D287-R260 D287-K256 E172-K281
H-J	D244-K339 R62-D294 K84-D400 K61-E153
I-J	E273-K403 E277-K403 K200-D386 R199-E145 R46-E174 K43-E276
J-U	D209-R147 R213-E131
a-C	D29-R66 E27-R220 E36-K308 E38-K308 E46-R329
a-E	D18-K327 D24-R329 E16-K319 R14-D312 K5-E219
b-G	D24-R220 D70-R373 D73-R118 E27-R220 E32-R220 E38-K308 E46-R329 E87-K355
b-I	D18-K327 D3-R220 E16-K319 R14-D312
b-F	D73-K200 R80-E232
b-E	K62-E53
c-D	E16-R329 E16-K319 R14-D312
d-F	D8-K308 E16-K319 R14-D312

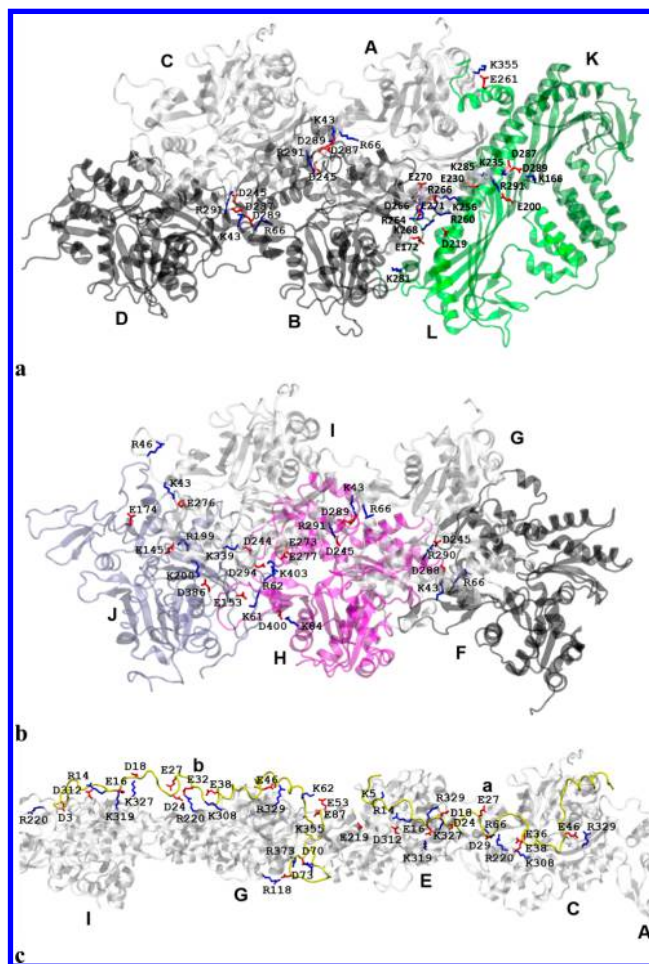


Figure 2. HBs and SBs forming charged residues at the intersubunit interfaces: (a) at the barbed end, (b) at the pointed end, and (c) between ER1/ER2 and ARP1 subunits. The color coding is the same as that in Figure 1. Acidic and basic residues are represented by side chains colored red and blue, respectively. The various subunits are labeled by the chain ids. Also see Tables 2 and 3.

explains why the pointed-end capping by ARP11 is favored over filament extension.³⁷ These capping interactions sequester residue K43 of ARP1 subunit I, so it cannot be recruited to bind another ARP1 via a key SB between K43 and D287³⁷ (see Table 3). Additionally, residues H65 and R66 (see Tables 2 and 3) in the subdomain 2 loop of ARP1 are absent in ARP11,³⁷ so they cannot be recruited to form a HB or SB with another ARP1 at the pointed end. In sum, our findings account for favorable capping of the pointed end by ARP11 and unfavorable addition of another ARP1. Taken together, the capping of the barbed and pointed ends permits the assembly of a dynactin filament with a defined length.

In the absence of p62, the ARP1 subunit is loosely associated with the p25 subunit (chain V) and the p27 subunit (chains U) via 3–5 HBs and ~1 SB in our simulations (see Table 1). Addition of p62 is expected to reinforce this loose association in MD simulations, which await future solution of a high-resolution structure for the p62 subunit.

In the cryo-EM structure of the dynactin filament,³⁷ two pairs of extended regions (ER1–2 and ER3–4) coat the filament surface, which correspond to the N termini of four p50 subunits.⁶⁵ ER1 and ER2 contact the top protofilament, with ER1 (chain a) running from subunit C to subunit E and ER2

(chain b) running from subunit G to subunit I (see Figure 1a). ER3 and ER4 reach down to contact the bottom protofilament, with ER3 (chain c) running from subunit B to subunit D and ER4 (chain d) contacting subunit F. On the basis of these observations, it was proposed that dynactin filament assembly is initiated by the four ERs recruiting eight ARP1 subunits and stabilizing their polymerization into a filament with five subunits on the top protofilament and three on the bottom protofilament (see Figure 1a). To test the proposal mentioned above, we examined the dynamic interactions between the four ERs and the ARP1 subunits during the MD simulations. ER1 and ER2 bind primarily with ARP1 subunits CEGI, featuring 12–23 HBs and ~4 SBs (see Table 1). Such strong HB and SB interactions can be attributed to numerous acidic residues in the ERs [including D3, D8, E16, D18, D24, E27, D29, E32, E36, E38, E46, D70, D73, and E87 (see Tables 2 and 3 and Figure 2c)] forming SBs with a positively charged groove on the ARP1 filament.^{37,65} These strong interactions allow ER1 and ER2 to readily recruit four ARP1 subunits and initiate the filament assembly process. Compared with ER1 and ER2, ER3 and ER4 are less structured, so they bind ARP1 subunits DF with fewer HBs and SBs (see Table 1). In agreement with our finding of differences between ER1–2 and ER3–4, a previous study⁶⁵ suggested that the two pairs of ERs experience different environments, with one pair (ER1–2) being more closely bound to the ARP1 filament.

In summary, our MD simulations revealed stronger intersubunit HB and SB interactions at the barbed and pointed ends of the ARP1 filament and between two ERs and the ARP1 subunits (compared with the interactions within the filament). These key interactions may energetically drive filament termination by the capping proteins (*CapZ $\alpha\beta$* at the barbed end and ARP11 at the pointed end) and the initial recruitment of the ARP1 subunits by the ERs, respectively.³⁷ Future mutational studies that target these interactions will be needed to validate their importance to dynactin filament assembly.

Electrostatics-Based Modeling of BICD2N Bound to Dynactin and the Dynein Tail. In the cryo-EM structure of TDB (PDB entry SAFU, chains 5 and 6), the BICD2N homodimer was modeled as two backbone traces of unknown amino acids because of the limited resolution (~8.2 Å³⁷). Therefore, this structure did not reveal how BICD2N interacts with dynactin and the dynein tail at the amino acid level. Here we used electrostatics-based modeling to define the unknown binding interface between BICD2N and dynactin and the dynein tail and identify key charged residues involved in the binding.

The ~270 residues of mouse BICD2N are predicted to form an α -helical coiled-coil structure that requires tight packing of core nonpolar residues at the *a/d* heptad positions. Meanwhile, BICD2N is rich in charged residues, with basic (acidic) residues accounting for 15% (22%) of all residues and a negative net charge. This charge richness resembles that of another well-studied coiled-coil protein α -tropomyosin [with basic (acidic) residues accounting for 19% (28%) of all 284 residues]. α -tropomyosin is known to form predominantly electrostatic interactions with an actin filament,⁶⁶ and actin is homologous to ARP1 in the dynactin filament. On the basis of the similarities described above, we hypothesize that BICD2N interacts electrostatically with the dynactin filament, although the BICD2N-binding sites on ARP1 are distinct from the tropomyosin-binding sites on actin.³⁷ Additionally, BICD2N and most subunits of the dynactin filament (except p25) have

negative net charges, so their charged residues must be placed at specific positions to achieve favorable electrostatic interaction between BICD2N and the dynactin filament.

By exploiting the key features of BICD2N mentioned above, we built a structural model of BICD2N as follows: (1) threading the mouse BICD2 sequence along the coiled-coil backbone traces of BICD2N (with a shift of residue position by $S \in [0, 100]$) and (2) finding an optimal threading solution that is both compatible with the coiled-coil structure and minimized in the electrostatic interaction energy between BICD2N and dynactin and dynein (see Methods). By attachment of a GFP to the N terminus of mouse BICD2 and visualization of it via cryo-EM, it was determined that the coiled coil of BICD2N starts near its N terminus.³⁷ Therefore, we focused our modeling near $S = 0$ (see Methods). In the optimized model where $S = 2$, amino acids 3–277 are assigned to the 275-amino acid coiled-coil structure of BICD2N in the TDB structure³⁷ (see Figure 3a).

On the basis of this model, we identified a key subset of BICD2 residues with a $\geq 5\%$ contribution to the electrostatic interaction energy [including E20*, K90*, E100*, and R164* in chain 5 and E25*, K40, E124*, R160*, E234, E237*, E241*, E242*, and E245* in chain 6 (see Figure 3a)], which interact with ARP1 subunit A, β -actin, p25, and the dynein tail (see Figure 3a). Most of these residues are conserved between BICD2 and its homologues BICD1 and BICD [labeled with an asterisk (see Figure S3)]. In dynactin, we found a cluster of three basic residues in p25 [K74, K75, and K78 (see Figure 3a)] prominently involved in binding of BICD2N, which are colocalized with known p25 sites of single-nucleotide variations linked to diseases (at amino acid positions 70, 72, and 73⁶⁷). The functional importance of p25 is further supported by the finding that it is a part of the conserved core of dynactin (the second most conserved subunit in dynactin after ARP1).⁶⁸ Additionally, p25 is the only dynactin subunit consistently showing alkaline pI (i.e., with a positive net charge), hinting at p25-specific electrostatic interactions within the dynactin complex or with other cellular components (such as negatively charged BICD2).⁶⁸ Three mutations linked to the dominant spinal muscular atrophy are mapped to BICD2N^{18,20,21} (including S107L, N188T, and I189F), and one of them (S107L) led to increased affinity for dynein and dynactin.²⁰ In our BICD2 model, S107 is located near E100, which is predicted to bind the dynein tail (see Figure 3a), so the S107L mutation may indirectly perturb the interaction between BICD2 and the dynein tail. N188 and I189 are located in the proximity of ARP11, so their mutations could affect the BICD2–ARP11 interactions.

In summary, our electrostatics-based modeling has predicted the charged residues involved in the electrostatic interaction of BICD2N with dynactin and dynein tail, which provide promising targets for future mutational studies.

Electrostatics-Based Modeling of Other BICD and BICD-Related Proteins Bound to Dynactin and the Dynein Tail. Next, we modeled three adaptor proteins that are sequentially similar to BICD2, including mouse BICD1¹⁴ (a mammalian orthologue of BICD2 with a 63% sequence identity), fruit fly BICD (a *Drosophila* orthologue of BICD2^{23,35} with a 39% sequence identity), and mouse BICD-related protein 1 (BICDR1).¹⁶ BICD2 and BICDR1 interact with dynein and dynactin with similar binding affinity despite the lack of significant sequence similarity.⁶⁹ Among these proteins, a highly conserved region was identified near the N

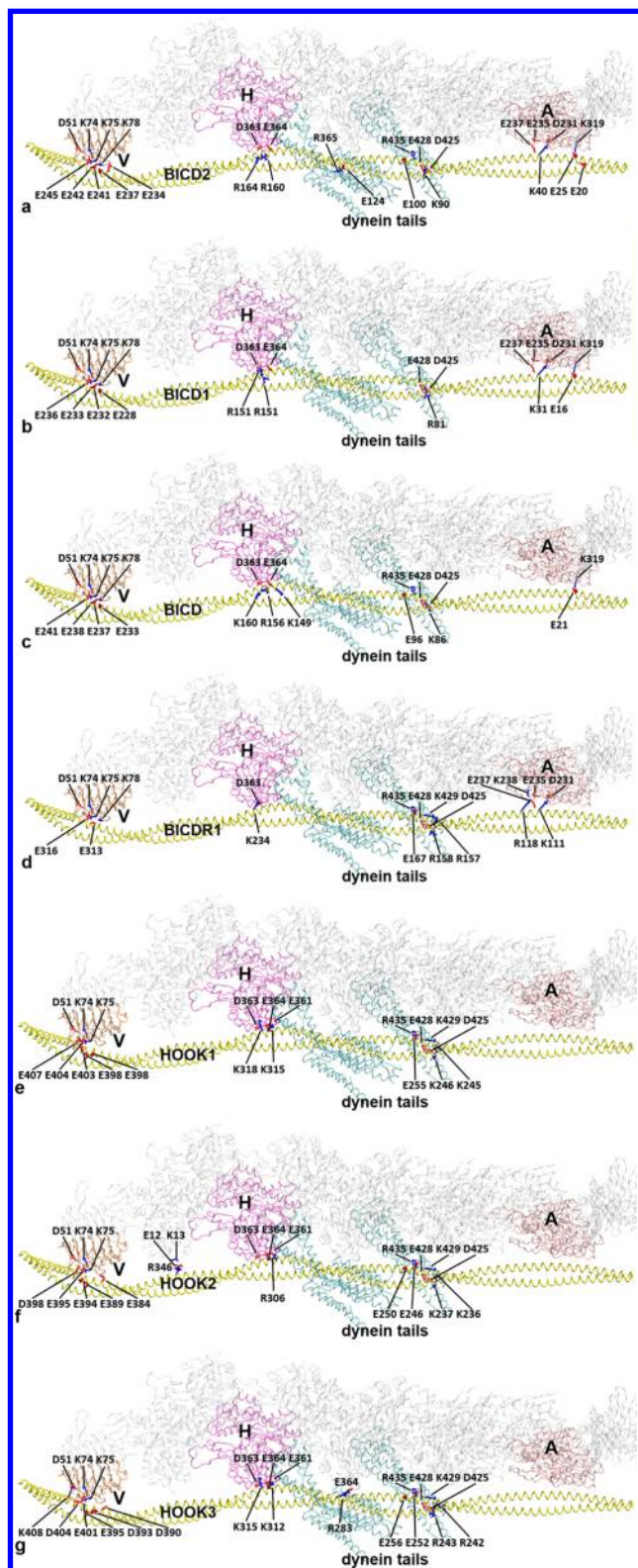


Figure 3. Models of the dynactin filament and dynein tails in complex with the following adaptor proteins: (a) BICD2, (b) BICD1, (c) BICD, (d) BICDR1, (e) HOOK1, (f) HOOK2, and (g) HOOK3. The following color coding is used: pink for ARP1-A, magenta for β -actin, orange for p25, yellow for coiled-coil adaptor protein, cyan for dynein tails, and gray for the rest of the filament. Acidic and basic residues involved in binding are represented by side chains colored red and blue, respectively. The three dynein subunits involved in binding are labeled by the chain ids.

terminus⁶⁹ (amino acids 35–50 of BICD, amino acids 30–45 of BICD1, amino acids 39–54 of BICD2, and amino acids 112–127 of BICDR1). The alignment in this region provides a useful constraint for the threading of these adaptor proteins (see below). We utilized the same protocol that was used for modeling BICD2 (see above), assuming the coiled-coil structure of BICD2N in the TDB structure³⁷ makes a good template for modeling the coiled-coil regions of BICD1, BICD, and BICDR1.

In the optimized model of BICD1 with the position shift $S = -7$, amino acids 1–268 of mouse BICD1 are assigned to amino acids 8–275 of the coiled-coil structure of BICD2N in the TDB structure.³⁷ On the basis of this model, we identified a subset of BICD1 residues (R81 and R151 in chain 5 and E16, K31, R151, E228, E232, E233, and E236 in chain 6) interacting with ARP1 subunit A, β -actin, p25, and the dynein tail (see Figure 3b).

In the optimized model of BICD with $S = -2$, amino acids 1–273 of *Drosophila* BICD are assigned to amino acids 3–275 of the coiled-coil structure. This model predicts a number of BICD residues (K86, E96, and K160 in chain 5 and E21, K149, R156, E233, E237, E238, and E241 in chain 6) interacting with ARP1 subunit A, β -actin, p25, and the dynein tail (see Figure 3c).

In the optimized model of BICDR1 with $S = 73$, amino acids 74–348 of mouse BICDR1 are assigned to the 275-amino acid coiled-coil structure. This model pinpoints a subset of BICDR1 residues (R157, R158, and E167 in chain 5 and K111, R118, K234, E313, and E316 in chain 6) interacting with ARP1 subunit A, β -actin, p25, and the dynein tail (see Figure 3d).

The binding sites of BICD1 and BICD are very similar to that of BICD2, which is consistent with their sequence alignments with BICD2 [with a shift of residue number by 9 and 4, respectively (see Figure S3)]. The binding sites of BICDR1 are also located in the same regions that contact p25, β -actin, ARP1 subunit A, and the dynein tail, although the corresponding residues cannot be aligned sequentially with the BICD proteins. Encouragingly, the models mentioned above consistently place the conserved N-terminal region in the proximity of ARP1 subunit A (see Figure 3b–d).

Mutations of two conserved N-terminal alanines (A43V/A44V in BICD2 and A116V/A117V in BICDR1) were shown to affect the interaction with the dynein–dynactin complex⁶⁹ (or affect the interactions within BICD⁷⁰). While these alanines do not directly contribute to binding in our electrostatics-based models, they are in the proximity of the predicted ARP1-binding residues in BICD2 [K40 (see Figure 3a)] and BICDR1 [K111 and R118 (see Figure 3d)], so their mutations may affect binding by structurally perturbing the ARP1-binding site or altering the flexibility of the coiled coil in a manner similar to that of the alanine clusters in tropomyosin.⁴⁵

In summary, our electrostatics-based modeling has identified key charged residues involved in the electrostatic interactions of three BICD and related proteins with dynactin and dynein tails, which are consistent with the sequence alignments and support the functional conservation of the binding sites.

Electrostatics-Based Modeling of the HOOK Proteins Bound to Dynactin and the Dynein Tail. Next, we modeled three adaptor proteins that are not sequentially similar to BICD2, including mouse HOOK1, HOOK2, and HOOK3. The HOOK proteins^{71,72} are involved in endocytic protein trafficking, Golgi organization, and cilium formation.^{73–78} Similar to BICD2, HOOK1 and HOOK3 were shown to enhance the formation of a dynein–dynactin complex and

processive dynein motility.⁷⁹ In addition to the central coiled-coil domain, the N-terminal domain of HOOK1 and HOOK3 (e.g., amino acids 1–160 of HOOK3) is also required for binding to dynactin and dynein.^{79,80} The three HOOK proteins are sequentially similar to each other, with the sequences of HOOK1 and HOOK2 (HOOK3) being 46% (57%) identical. We employed the same protocol that was used for modeling BICD2N, assuming the coiled-coil structure of BICD2N in the TDB structure³⁷ makes a good template for modeling the coiled-coil regions of the HOOK proteins despite the lack of sequence similarity.

In the optimized model of HOOK1, amino acids 162–436 are assigned to the 275-amino acid coiled-coil structure of BICD2N. This model predicts a subset of HOOK1 residues (K245, K246, E255, and E398 in chain 5 and K315, K318, E398, E403, E404, and E407 in chain 6) interacting with β -actin, p25, and the dynein tail (see Figure 3e).

In the optimized model of HOOK2, amino acids 153–427 are assigned to the coiled-coil structure. This model identifies a subset of HOOK2 residues (K236, K237, E246, E250, R346, and E389 in chain 5 and R306, E384, E394, E395, and D398 in chain 6) interacting with β -actin, p25, ARP11, and the dynein tail (see Figure 3f).

In the optimized model of HOOK3, amino acids 159–433 are assigned to the coiled-coil structure. This model pinpoints a subset of HOOK3 residues (R242, R243, E252, E256, and E395 in chain 5 and R283, K312, K315, D390, D393, E395, E401, D404, and K408 in chain 6) interacting with β -actin, p25, ARP1 subunit F, and the dynein tail (see Figure 3g).

The binding residues of three HOOK proteins are similar, which is consistent with their sequence alignments [with a shift of residue number by 9 (3) between HOOK1 and HOOK2 (HOOK3) (see Figure S4)]. Compared with the BICD proteins, the HOOK proteins share only the binding sites that contact p25, β -actin, and the dynein tail, but not ARP1. The loss of a common ARP1-binding site in HOOK proteins may lead to weak binding of dynactin to be compensated by the N-terminal domain forming new interactions with dynein and dynactin. The β -actin-binding site of HOOK proteins is in a central conserved region (amino acids 293–345 of HOOK3), which was shown to be functionally important by deletion mutations in a fungal homologue Hok1.⁷¹ In support of the key role of p25 in dynein and dynactin binding, it was shown that both dynein and p25 are required for the physical interaction between HookA (a homologue of human HOOK proteins) and dynein and dynactin.⁷²

In summary, our electrostatics-based modeling has pinpointed the charged residues involved in the electrostatic interactions of three HOOK proteins with dynactin and the dynein tail, which are consistent with their sequence alignments and differ from the BICD proteins in lacking a conserved ARP1-binding site.

CONCLUSION

In summary, we have employed molecular simulation and modeling to probe dynactin filament assembly and its interactions with cargo adaptor proteins at high resolution. First, we used MD simulation to analyze the dynamic intersubunit interactions in the dynactin filament. Our simulations revealed stronger intersubunit interactions at the barbed and pointed ends of the filament and involving the extended regions (compared with the intrafilament interactions), which may drive filament termination by the capping

proteins and recruitment of the actin-like proteins by the extended regions. Next, we modeled the unknown binding configuration between dynactin and the dynein tail and a number of coiled-coil adaptor proteins and predicted a key set of charged residues involved in the electrostatic interactions. Our models were validated in comparison with previous findings of conserved regions, functional sites, and disease mutations in the adaptor proteins and will provide a structural framework for guiding future functional and mutational studies of these key cargo-binding proteins.

ASSOCIATED CONTENT

Supporting Information

The Supporting Information is available free of charge on the ACS Publications website at DOI: 10.1021/acs.biochem.6b01002.

Comparison of the electrostatic binding energy and the binding affinity predicted by PRODIGY (Table S1), summary of intersubunit interactions based on last 10 ns of MD simulations (Table S2), score of coiled-coil packing and electrostatic energy (Figure S1), root-mean-square deviation of the core structure of the dynactin filament for three MD trajectories (Figure S2), multiple-sequence alignment of three BICD proteins (Figure S3), and multiple-sequence alignment of three HOOK proteins (Figure S4) (PDF)

AUTHOR INFORMATION

Corresponding Author

*Address: 239 Fronczak Hall, Buffalo, NY 14260. E-mail: wjzheng@buffalo.edu. Phone: (716) 645-2947. Fax: (716) 645-2507.

ORCID

Wenjun Zheng: 0000-0002-6236-9765

Funding

Supported by the American Heart Association (14GRNT18980033) and the National Science Foundation (0952736).

Notes

The author declares no competing financial interest.

ACKNOWLEDGMENTS

The simulations were conducted using the supercomputing cluster of the Center for Computational Research at the University at Buffalo and the Biowulf cluster at the National Institutes of Health.

REFERENCES

- (1) Gill, S. R., Schroer, T. A., Szilak, I., Steuer, E. R., Sheetz, M. P., and Cleveland, D. W. (1991) Dynactin, a conserved, ubiquitously expressed component of an activator of vesicle motility mediated by cytoplasmic dynein. *J. Cell Biol.* 115, 1639–1650.
- (2) McGrail, M., Gepner, J., Silvanovich, A., Ludmann, S., Serr, M., and Hays, T. S. (1995) Regulation of cytoplasmic dynein function in vivo by the Drosophila Glued complex. *J. Cell Biol.* 131, 411–425.
- (3) Plamann, M., Minke, P. F., Tinsley, J. H., and Bruno, K. S. (1994) Cytoplasmic dynein and actin-related protein Arp1 are required for normal nuclear distribution in filamentous fungi. *J. Cell Biol.* 127, 139–149.
- (4) McKenney, R. J., Huynh, W., Tanenbaum, M. E., Bhabha, G., and Vale, R. D. (2014) Activation of cytoplasmic dynein motility by dynactin-cargo adapter complexes. *Science* 345, 337–341.

- (5) Schlager, M. A., Hoang, H. T., Urnavicius, L., Bullock, S. L., and Carter, A. P. (2014) In vitro reconstitution of a highly processive recombinant human dynein complex. *EMBO J.* 33, 1855–1868.
- (6) King, S. J., and Schroer, T. A. (2000) Dynactin increases the processivity of the cytoplasmic dynein motor. *Nat. Cell Biol.* 2, 20–24.
- (7) Ross, J. L., Wallace, K., Shuman, H., Goldman, Y. E., and Holzbaur, E. L. (2006) Processive bidirectional motion of dynein-dynactin complexes in vitro. *Nat. Cell Biol.* 8, 562–570.
- (8) Kardon, J. R., Reck-Peterson, S. L., and Vale, R. D. (2009) Regulation of the processivity and intracellular localization of *Saccharomyces cerevisiae* dynein by dynactin. *Proc. Natl. Acad. Sci. U. S. A.* 106, 5669–5674.
- (9) Lees-Miller, J. P., Helfman, D. M., and Schroer, T. A. (1992) A vertebrate actin-related protein is a component of a multisubunit complex involved in microtubule-based vesicle motility. *Nature* 359, 244–246.
- (10) Schroer, T. A. (2004) Dynactin. *Annu. Rev. Cell Dev. Biol.* 20, 759–779.
- (11) Splinter, D., Razafsky, D. S., Schlager, M. A., Serra-Marques, A., Grigoriev, I., Demmers, J., Keijzer, N., Jiang, K., Poser, I., Hyman, A. A., Hoogenraad, C. C., King, S. J., and Akhmanova, A. (2012) BICD2, dynactin, and LIS1 cooperate in regulating dynein recruitment to cellular structures. *Mol. Biol. Cell* 23, 4226–4241.
- (12) Hoogenraad, C. C., Akhmanova, A., Howell, S. A., Dortland, B. R., De Zeeuw, C. I., Willemsen, R., Visser, P., Grosveld, F., and Galjart, N. (2001) Mammalian Golgi-associated Bicaudal-D2 functions in the dynein-dynactin pathway by interacting with these complexes. *EMBO J.* 20, 4041–4054.
- (13) Hoogenraad, C. C., Wulf, P., Schiefermeier, N., Stepanova, T., Galjart, N., Small, J. V., Grosveld, F., de Zeeuw, C. I., and Akhmanova, A. (2003) Bicaudal D induces selective dynein-mediated microtubule minus end-directed transport. *EMBO J.* 22, 6004–6015.
- (14) Dienstbier, M., and Li, X. (2009) Bicaudal-D and its role in cargo sorting by microtubule-based motors. *Biochem. Soc. Trans.* 37, 1066–1071.
- (15) Indran, S. V., Ballestas, M. E., and Britt, W. J. (2010) Bicaudal D1-dependent trafficking of human cytomegalovirus tegument protein pp150 in virus-infected cells. *J. Virol.* 84, 3162–3177.
- (16) Schlager, M. A., Kapitein, L. C., Grigoriev, I., Burzynski, G. M., Wulf, P. S., Keijzer, N., de Graaff, E., Fukuda, M., Shepherd, I. T., Akhmanova, A., and Hoogenraad, C. C. (2010) Pericentrosomal targeting of Rab6 secretory vesicles by Bicaudal-D-related protein 1 (BICDR-1) regulates neurogenesis. *EMBO J.* 29, 1637–1651.
- (17) Rudnik-Schoneborn, S., Deden, F., Eggermann, K., Eggermann, T., Wiczorek, D., Sellhaus, B., Yamoah, A., Goswami, A., Claeys, K. G., Weis, J., and Zerres, K. (2016) Autosomal dominant spinal muscular atrophy with lower extremity predominance: A recognizable phenotype of BICD2 mutations. *Muscle Nerve* 54, 496–500.
- (18) Rossor, A. M., Oates, E. C., Salter, H. K., Liu, Y., Murphy, S. M., Schule, R., Gonzalez, M. A., Scotto, M., Phadke, R., Sewry, C. A., Houlden, H., Jordanova, A., Tournev, I., Chamova, T., Litvinenko, I., Zuchner, S., Herrmann, D. N., Blake, J., Sowden, J. E., Acsadi, G., Rodriguez, M. L., Menezes, M. P., Clarke, N. F., Auer Grumbach, M., Bullock, S. L., Muntoni, F., Reilly, M. M., and North, K. N. (2015) Phenotypic and molecular insights into spinal muscular atrophy due to mutations in BICD2. *Brain* 138, 293–310.
- (19) Peeters, K., Litvinenko, I., Asselbergh, B., Almeida-Souza, L., Chamova, T., Geuens, T., Ydens, E., Zimon, M., Irobi, J., De Vriendt, E., De Winter, V., Ooms, T., Timmerman, V., Tournev, I., and Jordanova, A. (2013) Molecular defects in the motor adaptor BICD2 cause proximal spinal muscular atrophy with autosomal-dominant inheritance. *Am. J. Hum. Genet.* 92, 955–964.
- (20) Oates, E. C., Rossor, A. M., Hafezparast, M., Gonzalez, M., Spezziani, F., MacArthur, D. G., Lek, M., Cottenie, E., Scotto, M., Foley, A. R., Hurles, M., Houlden, H., Greensmith, L., Auer-Grumbach, M., Pieber, T. R., Strom, T. M., Schule, R., Herrmann, D. N., Sowden, J. E., Acsadi, G., Menezes, M. P., Clarke, N. F., Zuchner, S., Muntoni, F., North, K. N., and Reilly, M. M. (2013) Mutations in BICD2 cause dominant congenital spinal muscular atrophy and hereditary spastic paraplegia. *Am. J. Hum. Genet.* 92, 965–973.
- (21) Neveling, K., Martinez-Carrera, L. A., Holker, I., Heister, A., Verrips, A., Hosseini-Barkooie, S. M., Gilissen, C., Vermeer, S., Pennings, M., Meijer, R., te Riele, M., Frijns, C. J., Suchowersky, O., MacLaren, L., Rudnik-Schoneborn, S., Sinke, R. J., Zerres, K., Lowry, R. B., Lemmink, H. H., Garbes, L., Veltman, J. A., Schelhaas, H. J., Scheffer, H., and Wirth, B. (2013) Mutations in BICD2, which encodes a golgin and important motor adaptor, cause congenital autosomal-dominant spinal muscular atrophy. *Am. J. Hum. Genet.* 92, 946–954.
- (22) Martinez-Carrera, L. A., and Wirth, B. (2015) Dominant spinal muscular atrophy is caused by mutations in BICD2, an important golgin protein. *Front. Neurosci.* 9, 401.
- (23) Stuurman, N., Haner, M., Sasse, B., Hubner, W., Suter, B., and Aebi, U. (1999) Interactions between coiled-coil proteins: Drosophila lamin Dm0 binds to the bicaudal-D protein. *Eur. J. Cell Biol.* 78, 278–287.
- (24) Matanis, T., Akhmanova, A., Wulf, P., Del Nery, E., Weide, T., Stepanova, T., Galjart, N., Grosveld, F., Goud, B., De Zeeuw, C. I., Barnekow, A., and Hoogenraad, C. C. (2002) Bicaudal-D regulates COPI-independent Golgi-ER transport by recruiting the dynein-dynactin motor complex. *Nat. Cell Biol.* 4, 986–992.
- (25) Splinter, D., Tanenbaum, M. E., Lindqvist, A., Jaarsma, D., Flotho, A., Yu, K. L., Grigoriev, I., Engelsma, D., Haasdijk, E. D., Keijzer, N., Demmers, J., Fornerod, M., Melchior, F., Hoogenraad, C. C., Medema, R. H., and Akhmanova, A. (2010) Bicaudal D2, dynein, and kinesin-1 associate with nuclear pore complexes and regulate centrosome and nuclear positioning during mitotic entry. *PLoS Biol.* 8, e1000350.
- (26) Hodgkinson, J. L., Peters, C., Kuznetsov, S. A., and Steffen, W. (2005) Three-dimensional reconstruction of the dynactin complex by single-particle image analysis. *Proc. Natl. Acad. Sci. U. S. A.* 102, 3667–3672.
- (27) Imai, H., Narita, A., Maeda, Y., and Schroer, T. A. (2014) Dynactin 3D structure: implications for assembly and dynein binding. *J. Mol. Biol.* 426, 3262–3271.
- (28) Schafer, D. A., Gill, S. R., Cooper, J. A., Heuser, J. E., and Schroer, T. A. (1994) Ultrastructural analysis of the dynactin complex: an actin-related protein is a component of a filament that resembles F-actin. *J. Cell Biol.* 126, 403–412.
- (29) Eckley, D. M., Gill, S. R., Melkonian, K. A., Bingham, J. B., Goodson, H. V., Heuser, J. E., and Schroer, T. A. (1999) Analysis of dynactin subcomplexes reveals a novel actin-related protein associated with the arp1 minifilament pointed end. *J. Cell Biol.* 147, 307–320.
- (30) Imai, H., Narita, A., Schroer, T. A., and Maeda, Y. (2006) Two-dimensional averaged images of the dynactin complex revealed by single particle analysis. *J. Mol. Biol.* 359, 833–839.
- (31) Chowdhury, S., Ketcham, S. A., Schroer, T. A., and Lander, G. C. (2015) Structural organization of the dynein-dynactin complex bound to microtubules. *Nat. Struct. Mol. Biol.* 22, 345–347.
- (32) Yamashita, A., Maeda, K., and Maeda, Y. (2003) Crystal structure of CapZ: structural basis for actin filament barbed end capping. *EMBO J.* 22, 1529–1538.
- (33) Weisbrich, A., Honnappa, S., Jaussi, R., Okhrimenko, O., Frey, D., Jelesarov, I., Akhmanova, A., and Steinmetz, M. O. (2007) Structure-function relationship of CAP-Gly domains. *Nat. Struct. Mol. Biol.* 14, 959–967.
- (34) Yeh, T. Y., Kowalska, A. K., Scipioni, B. R., Cheong, F. K., Zheng, M., Derewenda, U., Derewenda, Z. S., and Schroer, T. A. (2013) Dynactin helps target Polo-like kinase 1 to kinetochores via its left-handed beta-helical p27 subunit. *EMBO J.* 32, 1023–1035.
- (35) Liu, Y., Salter, H. K., Holding, A. N., Johnson, C. M., Stephens, E., Lukavsky, P. J., Walshaw, J., and Bullock, S. L. (2013) Bicaudal-D uses a parallel, homodimeric coiled coil with heterotypic registry to coordinate recruitment of cargos to dynein. *Genes Dev.* 27, 1233–1246.
- (36) Terawaki, S., Yoshikane, A., Higuchi, Y., and Wakamatsu, K. (2015) Structural basis for cargo binding and autoinhibition of

Bicaudal-D1 by a parallel coiled-coil with homotypic registry. *Biochem. Biophys. Res. Commun.* 460, 451–456.

(37) Urnavicius, L., Zhang, K., Diamant, A. G., Motz, C., Schlager, M. A., Yu, M., Patel, N. A., Robinson, C. V., and Carter, A. P. (2015) The structure of the dynactin complex and its interaction with dynein. *Science* 347, 1441–1446.

(38) Bingham, J. B., and Schroer, T. A. (1999) Self-regulated polymerization of the actin-related protein Arp1. *Curr. Biol.* 9, 223–226.

(39) Yeh, T. Y., Quintyne, N. J., Scipioni, B. R., Eckley, D. M., and Schroer, T. A. (2012) Dynactin's pointed-end complex is a cargo-targeting module. *Mol. Biol. Cell* 23, 3827–3837.

(40) Eckley, D. M., and Schroer, T. A. (2003) Interactions between the evolutionarily conserved, actin-related protein, Arp11, actin, and Arp1. *Mol. Biol. Cell* 14, 2645–2654.

(41) Jacquot, G., Maidou-Peindara, P., and Benichou, S. (2010) Molecular and functional basis for the scaffolding role of the p50/dynamitin subunit of the microtubule-associated dynactin complex. *J. Biol. Chem.* 285, 23019–23031.

(42) Maier, K. C., Godfrey, J. E., Echeverri, C. J., Cheong, F. K., and Schroer, T. A. (2008) Dynamitin mutagenesis reveals protein-protein interactions important for dynactin structure. *Traffic* 9, 481–491.

(43) Karplus, M., and McCammon, J. A. (2002) Molecular dynamics simulations of biomolecules. *Nat. Struct. Biol.* 9, 646–652.

(44) Zheng, W., Hitchcock-DeGregori, S. E., and Barua, B. (2016) Investigating the effects of tropomyosin mutations on its flexibility and interactions with filamentous actin using molecular dynamics simulation. *J. Muscle Res. Cell Motil.* 37, 131–147.

(45) Zheng, W., Barua, B., and Hitchcock-DeGregori, S. E. (2013) Probing the flexibility of tropomyosin and its binding to filamentous actin using molecular dynamics simulations. *Biophys. J.* 105, 1882–1892.

(46) Stone, J. E., Hardy, D. J., Ufimtsev, I. S., and Schulten, K. (2010) GPU-accelerated molecular modeling coming of age. *J. Mol. Graphics Modell.* 29, 116–125.

(47) Caves, L. S., Evanseck, J. D., and Karplus, M. (1998) Locally accessible conformations of proteins: multiple molecular dynamics simulations of crambin. *Protein Sci.* 7, 649–666.

(48) Zhang, J., Yao, X., Fischer, L., Abenza, J. F., Penalva, M. A., and Xiang, X. (2011) The p25 subunit of the dynactin complex is required for dynein-early endosome interaction. *J. Cell Biol.* 193, 1245–1255.

(49) Fiser, A., and Sali, A. (2003) ModLoop: automated modeling of loops in protein structures. *Bioinformatics* 19, 2500–2501.

(50) Humphrey, W., Dalke, A., and Schulten, K. (1996) VMD: visual molecular dynamics. *J. Mol. Graphics* 14, 27–38.

(51) Martyna, G. J., Tobias, D. J., and Klein, M. L. (1994) Constant pressure molecular dynamics algorithms. *J. Chem. Phys.* 101, 4177–4189.

(52) Hoover, W. G. (1985) Canonical Dynamics - Equilibrium Phase-Space Distributions. *Phys. Rev. A: At, Mol., Opt. Phys.* 31, 1695–1697.

(53) Deserno, M., and Holm, C. (1998) How to mesh up Ewald sums. I. A theoretical and numerical comparison of various particle mesh routines. *J. Chem. Phys.* 109, 7678–7693.

(54) Ryckaert, J.-P., Ciccotti, G., and Berendsen, H. J. C. (1977) Numerical integration of the cartesian equations of motion of a system with constraints: molecular dynamics of n-alkanes. *J. Comput. Phys.* 23, 327–341.

(55) Phillips, J. C., Braun, R., Wang, W., Gumbart, J., Tajkhorshid, E., Villa, E., Chipot, C., Skeel, R. D., Kale, L., and Schulten, K. (2005) Scalable molecular dynamics with NAMD. *J. Comput. Chem.* 26, 1781–1802.

(56) MacKerell, A. D., Bashford, D., Bellott, M., Dunbrack, R. L., Evanseck, J. D., Field, M. J., Fischer, S., Gao, J., Guo, H., Ha, S., Joseph-McCarthy, D., Kuchnir, L., Kuczera, K., Lau, F. T. K., Mattos, C., Michnick, S., Ngo, T., Nguyen, D. T., Prodhom, B., Reiher, W. E., Roux, B., Schlenkerich, M., Smith, J. C., Stote, R., Straub, J., Watanabe, M., Wiorkiewicz-Kuczera, J., Yin, D., and Karplus, M. (1998) All-atom

empirical potential for molecular modeling and dynamics studies of proteins. *J. Phys. Chem. B* 102, 3586–3616.

(57) Mackerell, A. D., Jr., Feig, M., and Brooks, C. L., 3rd (2004) Extending the treatment of backbone energetics in protein force fields: limitations of gas-phase quantum mechanics in reproducing protein conformational distributions in molecular dynamics simulations. *J. Comput. Chem.* 25, 1400–1415.

(58) Jorgensen, W. L., Chandrasekhar, J., Madura, J. D., Impey, R. W., and Klein, M. L. (1983) Comparison of simple potential functions for simulating liquid water. *J. Chem. Phys.* 79, 926–935.

(59) Available at http://www.ch.embnet.org/software/COILS_form.html (accessed 8/9/2016).

(60) Available at <http://dunbrack.fccc.edu/scwrl4/> (downloaded 5/21/2011).

(61) Xue, L. C., Rodrigues, J. P., Kastriitis, P. L., Bonvin, A. M., and Vangone, A. (2016) PRODIGY: a web server for predicting the binding affinity of protein-protein complexes. *Bioinformatics* 32, 3676–3678.

(62) Kwiatek, O., Papa, I., Lebart, M. C., Benyamin, Y., and Roustan, C. (2000) Interaction of actin with the capping protein, CapZ from sea bass (*Dicentrarchus labrax*) white skeletal muscle. *Comp. Biochem. Physiol., Part B: Biochem. Mol. Biol.* 127, 551–562.

(63) Hug, C., Miller, T. M., Torres, M. A., Casella, J. F., and Cooper, J. A. (1992) Identification and characterization of an actin-binding site of CapZ. *J. Cell Biol.* 116, 923–931.

(64) Muhua, L., Karpova, T. S., and Cooper, J. A. (1994) A yeast actin-related protein homologous to that in vertebrate dynactin complex is important for spindle orientation and nuclear migration. *Cell* 78, 669–679.

(65) Cheong, F. K., Feng, L., Sarkeshik, A., Yates, J. R., 3rd, and Schroer, T. A. (2014) Dynactin integrity depends upon direct binding of dynamitin to Arp1. *Mol. Biol. Cell* 25, 2171–2180.

(66) Lorenz, M., Poole, K. J., Popp, D., Rosenbaum, G., and Holmes, K. C. (1995) An atomic model of the unregulated thin filament obtained by X-ray fiber diffraction on oriented actin-tropomyosin gels. *J. Mol. Biol.* 246, 108–119.

(67) See <https://hive.biochemistry.gwu.edu/tools/biomuta/biomuta.php?gene=DCTN5> (accessed 8/9/2016).

(68) Hammesfahr, B., and Kollmar, M. (2012) Evolution of the eukaryotic dynactin complex, the activator of cytoplasmic dynein. *BMC Evol. Biol.* 12, 95.

(69) Schlager, M. A., Serra-Marques, A., Grigoriev, I., Gumy, L. F., Esteves da Silva, M., Wulf, P. S., Akhmanova, A., and Hoogenraad, C. C. (2014) Bicaudal d family adaptor proteins control the velocity of Dynein-based movements. *Cell Rep.* 8, 1248–1256.

(70) Larsen, K. S., Xu, J., Cermelli, S., Shu, Z., and Gross, S. P. (2008) BicaudalD actively regulates microtubule motor activity in lipid droplet transport. *PLoS One* 3, e3763.

(71) Bielska, E., Schuster, M., Roger, Y., Berepiki, A., Soanes, D. M., Talbot, N. J., and Steinberg, G. (2014) Hook is an adapter that coordinates kinesin-3 and dynein cargo attachment on early endosomes. *J. Cell Biol.* 204, 989–1007.

(72) Zhang, J., Qiu, R., Arst, H. N., Jr., Penalva, M. A., and Xiang, X. (2014) HookA is a novel dynein-early endosome linker critical for cargo movement in vivo. *J. Cell Biol.* 204, 1009–1026.

(73) Maldonado-Báez, L., Cole, N. B., Kramer, H., and Donaldson, J. G. (2013) Microtubule-dependent endosomal sorting of clathrin-independent cargo by Hook1. *J. Cell Biol.* 201, 233–247.

(74) Baron Gaillard, C. L., Pallesi-Pocachard, E., Massey-Harroche, D., Richard, F., Arsanto, J. P., Chauvin, J. P., Lecine, P., Kramer, H., Borg, J. P., and Le Bivic, A. (2011) Hook2 is involved in the morphogenesis of the primary cilium. *Mol. Biol. Cell* 22, 4549–4562.

(75) Ge, X., Frank, C. L., Calderon de Anda, F., and Tsai, L. H. (2010) Hook3 interacts with PCMI to regulate pericentriolar material assembly and the timing of neurogenesis. *Neuron* 65, 191–203.

(76) Walenta, J. H., Didier, A. J., Liu, X., and Kramer, H. (2001) The Golgi-associated hook3 protein is a member of a novel family of microtubule-binding proteins. *J. Cell Biol.* 152, 923–934.

(77) Kramer, H., and Phistry, M. (1999) Genetic analysis of hook, a gene required for endocytic trafficking in drosophila. *Genetics* 151, 675–684.

(78) Kramer, H., and Phistry, M. (1996) Mutations in the Drosophila hook gene inhibit endocytosis of the boss transmembrane ligand into multivesicular bodies. *J. Cell Biol.* 133, 1205–1215.

(79) Olenick, M. A., Tokito, M., Boczkowska, M., Dominguez, R., and Holzbaaur, E. L. (2016) Hook Adaptors Induce Unidirectional Processive Motility by Enhancing the Dynein-Dynactin Interaction. *J. Biol. Chem.* 291, 18239–18251.

(80) Schroeder, C. M., and Vale, R. D. (2016) Assembly and activation of dynein-dynactin by the cargo adaptor protein Hook3. *J. Cell Biol.* 214, 309–318.